

Multivalley spin relaxation in the presence of high in-plane electric fields in n -type GaAs quantum wells

P. Zhang,^{1,2} J. Zhou,² and M. W. Wu^{1,2,*}

¹*Hefei National Laboratory for Physical Sciences at Microscale,
University of Science and Technology of China, Hefei, Anhui, 230026, China*

²*Department of Physics, University of Science and Technology of China, Hefei, Anhui, 230026, China*
(Dated: November 3, 2018)

Multi-valley spin relaxation in n -type GaAs quantum wells with in-plane electric field is investigated at high temperature by means of kinetic spin Bloch equation approach. The spin relaxation time first increases and then decreases with electric field, especially when the temperature is relatively low. We show that L valleys play the role of a “drain” of the total spin polarization due to the large spin-orbit coupling in L valleys and the strong Γ - L inter-valley scattering, and thus can enhance spin relaxation of the total system effectively when the in-plane electric field is high. Under electric field, spin precession resulting from the electric-field-induced magnetic field is observed. Meanwhile, due to the strong Γ - L inter-valley scattering as well as the strong inhomogeneous broadening in L valleys, electron spins in L valleys possess almost the same damping rate and precession frequency as those in Γ valley. This feature still holds when a finite static magnetic field is applied in Voigt configuration, despite that the g -factor of L valleys is much larger than that of Γ valley. Moreover, it is shown that the property of spin precession of the whole system is dominated by electrons in Γ valley. Temperature, magnetic field, and impurity can affect spin relaxation in low electric field regime. However, they are shown to have marginal influence in high electric field regime.

PACS numbers: 72.25.Rb, 72.20.Ht, 71.10.-w, 67.57.Lm

I. INTRODUCTION

The ability to manipulate electron spin degree of freedom in semiconductors has become an important issue for the realization of spintronic devices.^{1,2,3} Usual ways to manipulate spins are proposed by directly applying magnetic field or exploiting the spin-orbit interaction through a gate voltage^{4,5,6} and/or strain field.^{7,8,9,10} In addition, applying a drift electric field also provides an approach to manipulate spin, by which the dependence of spin-orbit coupling on electron momentum is exploited and an effective magnetic field can be induced.¹¹ However, these manipulations also affect spin relaxation and dephasing (R&D) time,^{10,11,12,13,14} which is an essential time scale for the design of spin-based devices. Moreover, as the goal of semiconductor spintronics is to combine “traditional” semiconductor electronics with the utilization of the spin state and most current electronic devices are performed at high-field transport condition, the study of drift electric field on spin R&D is therefore essential.

Earlier Monte-Carlo simulation has revealed that the drift electric field can enhance spin relaxation in GaAs quantum wires^{12,13} and bulk material.¹⁴ However, these studies fail to treat all scattering, especially the Coulomb scattering, completely. It was pointed out that the Coulomb scattering can also cause spin R&D.^{15,16} Investigations based on fully microscopic kinetic spin Bloch equation (KSBE) approach^{17,18} have demonstrated that the Coulomb scattering is very important to the spin R&D.^{11,15,19,20,21} This has also been verified experimentally.^{22,23,24} Among these works, Ref. 11 gives a complete understanding of the hot-electron effect on spin R&D in n -type GaAs quantum wells (QWs),

where all the scattering is explicitly included and calculated self-consistently. It is shown that the spin R&D increase with electric field at high temperature, but decrease with it at low temperature.¹¹ Nevertheless, due to the lowest-subband used in the investigation and the “runaway effect”,²⁵ that study is limited to electric field lower than 1 kV/cm.¹¹ When the electric field is further raised, the multi-subband or even the multi-valley effect should be taken into account.²⁰ In Ref. 20, the electric field has been raised up to 3 kV/cm and the multi-subband scattering is considered. It is shown that the spin R&D first decrease then increase with the applied electric field at low temperature.²⁰ These effects^{8,20} have very recently been demonstrated by Holleitner *et al.* experimentally.²⁶ However, when the electric field is further increased, the inter-valley scattering should be taken into account.

The inter-valley scattering can lead to interesting phenomena, such as the charge Gunn effect in GaAs,²⁷ which comes from the different mobilities in different valleys due to the different effective masses. Studies focusing on scattering and transport between different valleys without the spin degree of freedom have been performed long time ago.^{28,29,30,31,32} When spin is considered, the different spin-orbit couplings and the different effective g -factors, together with the well known different momentum relaxations at different valleys may lead to complex spin R&D phenomena. Spin injection through a Schottky barrier into bulk GaAs, with Γ - L - X valley structure included, has been studied by Monte-Carlo simulation, revealing faster decay of current (electron) spin polarization in the upper valleys.³³ Recently, a spin Gunn effect has been proposed, depicting a process of spontaneous

spin-polarization amplification in semiconductors such as GaAs.³⁴ However, as this effect is predicted to happen in the high-electric-field charge Gunn domain, and the condition for it depends strongly on spin relaxation time, it is necessary to investigate spin relaxation under high electric field.

In this work, we perform a fully microscopic investigation on spin relaxation with high in-plane electric field at high temperature in n -type GaAs QWs, with Γ and L valleys included. The spin relaxation comes from the D'yakonov-Perel' mechanism.³⁵ This paper is organized as follows. In Sec. II, we set up the model and construct the KSBES. We present our main results in Sec. III, including the role of inter-valley scattering, the spin precession properties, and the effects of temperature, magnetic field, and impurity on spin R&D. We summarize in Sec. IV.

II. MODEL AND KSBES

We start our investigation from an n -type GaAs [001] QW with well width a . The growth direction is assumed along z -axis. Γ valley is located at the center of the Brillouin zone and four L valleys are at $\mathbf{K}_{L_i}^0 = (\pi/a_0)(1, \pm 1, \pm 1)$ that are rotationally symmetric around the [100] (x) axis, with a_0 denoting the lattice constant and $i = 1, \dots, 4$. Under spherically symmetric approximation, the effective electron masses of Γ and L valleys are $m_\Gamma = 0.067m_0$ and $m_{L_i} = m_L = 0.230m_0$,^{28,36} where m_0 is the free-electron mass. Assuming parabolic and isotropic band structure for each valley, the electron energy at the bottom of each valley reads³⁰

$$\varepsilon_{\mathbf{k}_\Gamma} = \frac{\hbar^2 \mathbf{k}_\Gamma^2}{2m_\Gamma}, \quad (1)$$

$$\varepsilon_{\mathbf{k}_{L_i}} = \frac{\hbar^2 \mathbf{k}_{L_i}^2}{2m_L} + \varepsilon_{\Gamma L}, \quad (2)$$

where \mathbf{k}_λ is the x - y -plane projection of the three-dimensional relative momentum $\mathbf{K} - \mathbf{K}_\lambda^0$ ($\lambda = \Gamma, L_i$), with the electron energy at \mathbf{K}_λ^0 set as the reference point. $\varepsilon_{\Gamma L}$ is the effective Γ - L energy difference in the two-dimensional structure: $\varepsilon_{\Gamma L} = E_{\Gamma L} - \frac{\hbar^2 \pi^2}{2a^2} (\frac{1}{m_\Gamma} - \frac{1}{m_L})$, where $E_{\Gamma L} = 0.28$ eV is the Γ - L energy difference in bulk.³⁷ Here an infinite-well-depth assumption is used. a is set as 7.5 nm throughout the paper. $\varepsilon_{\Gamma L} = 0.21$ eV is smaller than the energy difference of the lowest two subbands of the Γ valley, which is about 0.30 eV. It is also noted that the effective L - X energy difference in this two dimensional structure is as high as 0.17 eV when the spherical effective mass of X valleys is about $0.6m_0$.³⁶ Thus in this work, only the lowest subbands of Γ and L valleys are considered.

The Hamiltonian of the system reads

$$H = \sum_{\lambda} H_{\lambda}^0 + \sum_{\lambda\lambda'} H_{\lambda\lambda'}^I, \quad (3)$$

$$H_{\lambda\lambda'}^I = H_{\lambda\lambda'}^{e-e} + H_{\lambda\lambda'}^{e-p} + H_{\lambda\lambda'}^{e-i} \delta_{\lambda\lambda'}. \quad (4)$$

Here

$$H_{\lambda}^0 = \sum_{\mathbf{k}_\lambda \sigma \sigma'} \left\{ (\varepsilon_{\mathbf{k}_\lambda} + e\mathbf{E} \cdot \mathbf{R}) \delta_{\sigma\sigma'} + \left[\frac{1}{2} g_{\lambda} \mu_B \mathbf{B} + \mathbf{h}_{\lambda}(\mathbf{k}_{\lambda}) \right] \cdot \boldsymbol{\sigma}_{\sigma\sigma'} \right\} C_{\mathbf{k}_\lambda \sigma}^{\dagger} C_{\mathbf{k}_\lambda \sigma'} \quad (5)$$

is the free electron Hamiltonian at λ valley, where $-e$ is the electron charge, $\mathbf{R} = (x, y)$ is the position of the electron, \mathbf{E} is the electric field (the system is assumed to be spacial homogeneous one so that \mathbf{E} does not depend on the position), \mathbf{B} is the magnetic field in Voigt configuration and $\boldsymbol{\sigma}$ is Pauli matrices. In the calculation, \mathbf{E} and \mathbf{B} are taken along x -axis unless otherwise specified. $C_{\mathbf{k}_\lambda \sigma}^{\dagger} (C_{\mathbf{k}_\lambda \sigma})$ is the creation (annihilation) operator for electron with relative wave vector \mathbf{k}_λ and spin σ . The effective g -factors are $g_{\Gamma} = -0.44$ ³⁸ and $g_{L_i} = g_L = 1.77$.³⁹ $\mathbf{h}_{\lambda}(\mathbf{k})$ represents the Dresselhaus spin-orbit coupling.⁴⁰ In the coordinate system adopted in this work,⁴¹

$$h_{\Gamma}(\mathbf{k}_{\Gamma}) = \frac{\gamma}{2} (k_{\Gamma x} (k_{\Gamma y}^2 - \langle k_{\Gamma z}^2 \rangle), k_{\Gamma y} (\langle k_{\Gamma z}^2 \rangle - k_{\Gamma x}^2), \langle k_{\Gamma z}^2 \rangle (k_{\Gamma x}^2 - k_{\Gamma y}^2)), \quad (6)$$

$$h_{L_i}(\mathbf{k}_{L_i}) = \beta (k_{L_i x}, k_{L_i y}, \langle k_{L_i z}^2 \rangle) \times \hat{\mathbf{n}}_i. \quad (7)$$

Here $\hat{\mathbf{n}}_i$ is the unit vector along the longitudinal principle axis of L_i valley. $\langle k_{\lambda z}^2 \rangle$ ($\langle k_{\lambda z}^2 \rangle$) represents the average of the operator $-i\partial/\partial z - K_{\lambda z}^0$ [$(-i\partial/\partial z - K_{\lambda z}^0)^2$] over the electron state of the lowest subband in λ valley. With the infinite-depth assumption, it reads $\langle k_{\lambda z}^2 \rangle = 0$ [$\langle k_{\lambda z}^2 \rangle = (\pi/a)^2$]. The spin-orbit coupling coefficients utilized in the calculation are $\gamma = 0.011$ eV \cdot nm^{321,42} and $\beta = 0.026$ eV \cdot nm,⁴³ respectively. The interaction Hamiltonian is composed of the intra- ($\lambda' = \lambda$) and inter-valley ($\lambda' \neq \lambda$) Coulomb scattering $H_{\lambda\lambda'}^{e-e}$, electron-phonon scattering $H_{\lambda\lambda'}^{e-p}$ and electron-impurity scattering $H_{\lambda\lambda'}^{e-i}$. Expressions of these Hamiltonian can be found in books^{44,45} and Refs. 28,46.

The KSBES constructed by the nonequilibrium Green's function method read^{17,18}

$$\dot{\rho}_{\mathbf{k}_\lambda} = \dot{\rho}_{\mathbf{k}_\lambda}|_{dri} + \dot{\rho}_{\mathbf{k}_\lambda}|_{coh} + \sum_{\lambda'} \dot{\rho}_{\mathbf{k}_\lambda}|_{scat, \lambda\lambda'}. \quad (8)$$

Here $\rho_{\mathbf{k}_\lambda}$ represent the density matrices of electrons with relative momentum \mathbf{k}_λ in valley λ , whose diagonal terms $\rho_{\mathbf{k}_\lambda, \sigma\sigma} \equiv f_{\mathbf{k}_\lambda, \sigma}$ ($\sigma = \pm 1/2$) represent the electron distribution functions and the off-diagonal ones $\rho_{\mathbf{k}_\lambda, \frac{1}{2} - \frac{1}{2}} = \rho_{\mathbf{k}_\lambda, -\frac{1}{2} \frac{1}{2}}^*$ describe the inter-spin-band correlations for the spin coherence. $\dot{\rho}_{\mathbf{k}_\lambda}|_{dri} = e\mathbf{E} \cdot \nabla_{\mathbf{k}_\lambda} \rho_{\mathbf{k}_\lambda}$ are the driving terms from the external electric field. $\dot{\rho}_{\mathbf{k}_\lambda}|_{coh}$ are the coherent terms describing the coherent spin precessions and $\dot{\rho}_{\mathbf{k}_\lambda}|_{scat, \lambda\lambda'}$ stand for the intra- ($\lambda = \lambda'$) and inter-valley ($\lambda \neq \lambda'$) scattering terms. Expressions of these terms are given in Appendix A.

The initial conditions at time $t=0$ are prepared from spin unpolarized equilibrium states (in the absence of electric field) at time $t = -t_0$:

$$f_{\mathbf{k}_\Gamma, \sigma}(-t_0) = \{ \exp[(\varepsilon_{\mathbf{k}_\Gamma} - \mu)/k_B T] + 1 \}^{-1}, \quad (9)$$

$$f_{\mathbf{k}_{L_i}, \sigma}(-t_0) = \rho_{\mathbf{k}_\Gamma, \frac{1}{2} - \frac{1}{2}}(-t_0) = \rho_{\mathbf{k}_{L_i}, \frac{1}{2} - \frac{1}{2}}(-t_0) = 0 \quad (10)$$

with μ representing the chemical potential at temperature T . We turn on the electric field at $t = -t_0$ and allow the system to evolve to the steady state before $t = 0$. Under the driving field and the inter-valley scattering, part of electrons in Γ valley are driven to L valleys. Then we turn on a circularly polarized laser pulse with width $\delta_\tau = 0.01$ ps at $t = 0$ to excite spin-up electron with Gaussian-like distribution to Γ valley: $\delta f_{\mathbf{k}_\Gamma, 1/2} = \alpha \exp[-(\varepsilon_{\mathbf{k}_\Gamma} - \varepsilon_F)^2 / 2\delta_\varepsilon^2] [1 - f_{\mathbf{k}_\Gamma, 1/2}(0)]$. Here $\alpha = NP_0 / \{\sum_{\mathbf{k}_\Gamma} \exp[-(\varepsilon_{\mathbf{k}_\Gamma} - \varepsilon_F)^2 / 2\delta_\varepsilon^2] [1 - f_{\mathbf{k}_\Gamma, 1/2}(0)]\}$, ε_F is the Fermi energy of Γ valley and $\delta_\varepsilon = \hbar / \delta_\tau$. N is the total electron density after the pulse excitation and P_0 is the spin polarization excited by the pulse. In this work, $N = 4 \times 10^{11} \text{ cm}^{-2}$ and $P_0 = 5\%$.

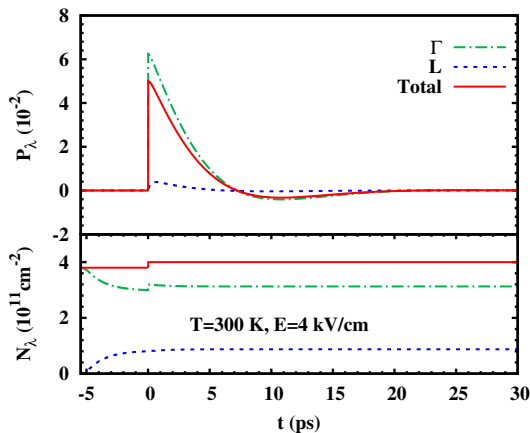


FIG. 1: (Color online) A typical time evolution of the initial steady-state preparation (density N_λ and spin polarization P_λ) under the electric field $E = 4$ kV/cm and a spin-polarization generation by a laser pulse at $t = 0$. $N_i = B = 0$. Chain curves: Γ valley; Dashed curves: L valleys; Solid curves: the total.

III. NUMERICAL RESULTS

We numerically solve the KSBEs following the scheme mainly laid out in Ref. 11, with extension to the inter-valley scattering given in Appendix B. In Fig. 1 we show a typical time evolution of the initial steady-state preparation under the influence of the electric field and a spin-polarization generation by a laser pulse. The electric field is applied from time $t = -t_0 = -5.5$ ps, and the laser pulse is applied at $t = 0$ ps. $P_\lambda(t) \equiv 2 \sum_{\mathbf{k}_\lambda \sigma} [\sigma f_{\mathbf{k}_\lambda, \sigma}(t)] / \sum_{\mathbf{k}_\lambda \sigma} f_{\mathbf{k}_\lambda, \sigma}(t)$ and $N_\lambda(t) \equiv \sum_{\mathbf{k}_\lambda \sigma} f_{\mathbf{k}_\lambda, \sigma}(t)$ are the spin polarization and the electron density at λ valley, separately. The steady-state drift velocity of λ valley \mathbf{v}_λ can be obtained from the steady value of $\mathbf{v}_\lambda(t) \equiv \sum_{\mathbf{k}_\lambda \sigma} [f_{\mathbf{k}_\lambda, \sigma}(t) \hbar \mathbf{k}_\lambda / m_\lambda] / \sum_{\mathbf{k}_\lambda \sigma} f_{\mathbf{k}_\lambda, \sigma}(t)$. The steady-state drift velocities v_λ of each valley as well as the total drift velocity against the electric field E are plotted in Fig. 2. From the figure the negative differ-

ential electric conductance of the total drift velocity is obtained.

The hot-electron temperature T_e can be obtained by fitting the Boltzmann tail of the calculated steady-state electron distribution of each valley.¹¹ Our results show that each valley has its own hot-electron temperature(s). Moreover, for Γ valley, there are two temperatures. One is at the energy regime which overlaps with that of L valleys. In this regime, electrons at Γ and L valleys share the *same* hot-electron temperature (labeled as T_L) due to the strong inter-valley scattering. The other is T_Γ for electrons in the lower energy regime of Γ valley. That is the typical hot-electron temperature of Γ valley and is higher than T_L . T_Γ and T_L as functions of electric field at different lattice temperatures are plotted in Fig. 3. It shows that electrons with smaller effective mass (such as those of Γ valley) and lower lattice temperature (thus relatively weak scattering) are easier to be accelerated and heated.

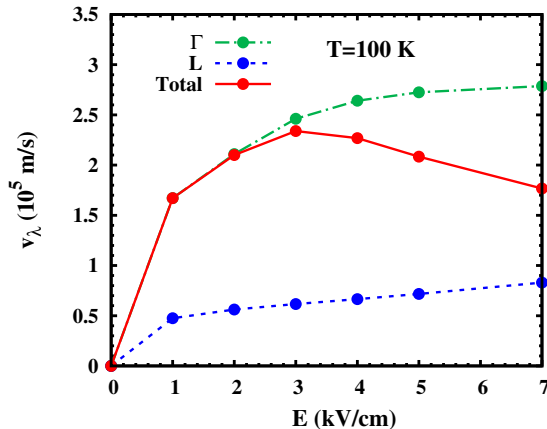


FIG. 2: (Color online) Steady-state drift velocity v_λ against electric field E at $T=100$ K. $N_i = B = 0$. Chain curve: Γ valley; Dashed curve: L valleys; Solid curve: the total.

The spin relaxation time τ can be obtained from the temporal evolution of spin polarization P_λ . Due to the lowest conduction subbands used in each valley and the “run-away” effect,²⁵ our research is limited to electric field up to 7 kV/cm.

A. Temporal evolution of spin polarization

We first show the temporal evolutions of total spin polarization $P_{Total}(t) \equiv \sum_\lambda P_\lambda(t)$ under different electric fields at $T = 200$ K with $B = N_i = 0$ in Fig. 4. The corresponding spin relaxation times obtained from the calculations are also given in the figure caption. It is seen from the figure that in the presence of electric field, electron spins precess with the precession period showing E -dependence. This is because the center-of-mass

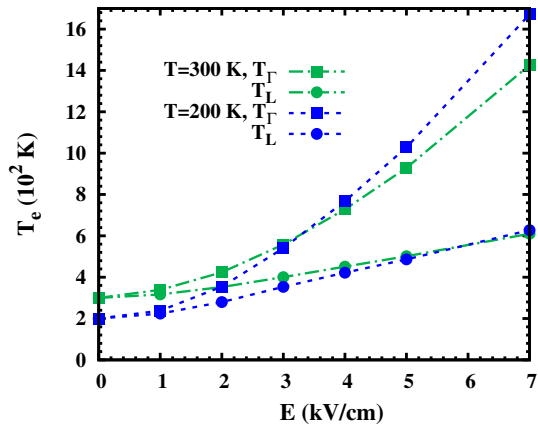


FIG. 3: (Color online) Hot-electron temperature T_Γ (curves with squares) and T_L (curves with circles) against electric field E at lattice temperature $T=300$ K (chain curves) and 200 K (dashed curves). $N_i = B = 0$.

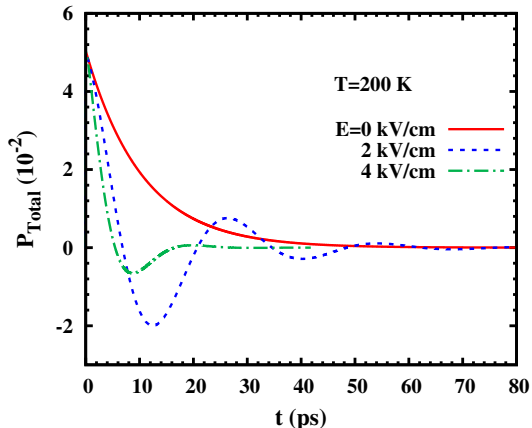


FIG. 4: (Color online) Temporal evolution of spin polarization P_{Total} when $E = 0$ (solid curve), 2 (dashed curve), and 4 kV/cm (chain curve). The corresponding spin relaxation times are fitted to be 10.5, 14.4, and 4.7 ps, respectively. $N_i = B = 0$.

momentum induced by the electric field leads to an effective magnetic field via the Dresselhaus spin-orbit coupling Eqs. (6) and (7).¹¹ Another interesting phenomenon is that the spin relaxation first decreases and then increases with electric field. It is known that the electric field can cause two effects: hot-electron effect and center-of-mass drift effect.¹¹ The hot-electron effect increases the inhomogeneous broadening as well as the scattering. The joint effects lead to enhanced (reduced) spin R&D in weak (strong) scattering limit,^{21,47} when the linear Dresselhaus term of the Γ valley is important.²⁰ The second effect forces spins to precess around the induced magnetic field mentioned previously and hence reduces the inhomogeneous broadening and the spin R&D. However, this

effect is quite marginal compared to the first one.¹¹ It has been demonstrated before that electrons in Γ valley is in the strong scattering limit.^{11,21,47} When the electric field is low, electrons are mainly distributed in the Γ valley. Thus the influence of hot-electron effect in the strong scattering limit causes τ to increase with E . However, when the electric field is high enough, apart from the fact that the increase of inhomogeneous broadening from the cubic term of the Dresselhaus term in Γ valley becomes important,²⁰ L valleys also start to play an important role. The amount of electrons sitting in L valleys grows with the electric field and the hot-electron temperature increases with the field as well. Thus the inter-valley scattering becomes more important with the increase of electric field. The strong spin-orbit coefficient at L valleys in conjunction with the inter-valley scattering lead to the decrease of the spin relaxation time with the field.

B. Effect of inter-valley scattering on spin relaxation

To elucidate the effect of inter-valley scattering on spin relaxation, we compare the spin relaxation under four different conditions: (a) with both Γ - L inter-valley Coulomb and electron-phonon scattering, (b) with Γ - L inter-valley Coulomb scattering $H_{\Gamma-L}^{e-e}$ only, (c) with Γ - L inter-valley electron-phonon scattering $H_{\Gamma-L}^{e-p}$ only and (d) without any Γ - L inter-valley scattering. (It is stressed that besides $H_{\Gamma-L}^{e-e}$ and $H_{\Gamma-L}^{e-p}$, all the other scattering terms are always present.) In order to get a clear insight into the inter-valley scattering to the spin relaxation, we need to prepare enough electron density and spin polarization in the L -valleys. To do so, we first switch off the coherent terms at time $t = 0$ (or even at $t = -t_0$, both yield the same result where there is no spin polarization) and allow the system to evolve to a spin polarized steady state (typically, the time t_r needed to reach a steady spin polarization is about 6 ps after the circularly polarized laser pulse is applied when $T = 300$ K, $E = 2$ kV/cm, and $B = N_i = 0$). It is noted that all inter-valley scattering should be included at this stage in order to allow Γ electrons enter into L valleys, driven by the electric field. Then we switch on the coherent terms to allow spin precession and switch off the corresponding Γ - L inter-valley scattering at time t_r . One should keep in mind that in our full calculation [such as under condition (a)], the coherent terms and all the scattering terms are present at all the time.

In Fig. 5 we plot time evolution of $|P_\lambda|$ against $t - t_r$ starting from the moment when the spin relaxation begins. t_r is taken as 0 for condition (a). In the calculation, $T = 300$ K, $E = 2$ kV/cm and $B = N_i = 0$. From Fig. 5(a), one can see that in the real situation, Γ and L valleys share almost the identical damping rate and precession period in spin precession, although the initial spin polarization of L valleys is very small. How-

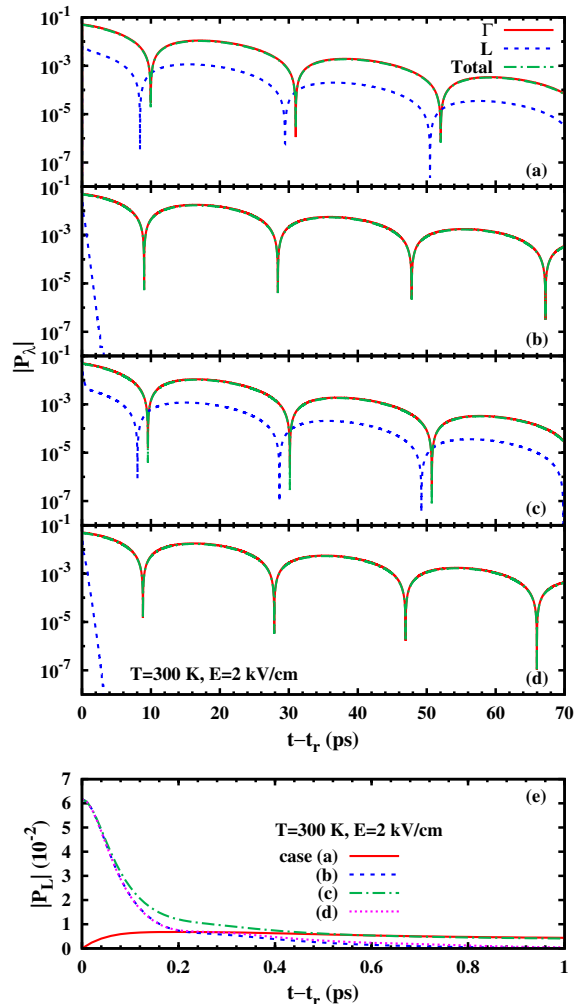


FIG. 5: (Color online) Spin polarization $|P_\lambda|$ vs. $t - t_r$ under electric field $E = 2$ kV/cm. Solid curve: Γ valley; dashed curve: L valley; and chain curve: the total. (a): with both $H_{\Gamma-L}^{e-p}$ and $H_{\Gamma-L}^{e-e}$; (b): without $H_{\Gamma-L}^{e-p}$; (c): without $H_{\Gamma-L}^{e-e}$; and (d): without $H_{\Gamma-L}^{e-e}$ and $H_{\Gamma-L}^{e-p}$. $T = 300$ K and $N_i = B = 0$. (e): The initial time evolution of spin polarization of L valleys.

ever, when $H_{\Gamma-L}^{e-p}$ is absent, *huge* differences between spin relaxations in Γ and L valleys appear: Despite whether $H_{\Gamma-L}^{e-e}$ is present [Fig. 5(b)] or absent [Fig. 5(d)], the spin relaxation in L valleys is much faster than that in Γ valley, regardless of much larger initial spin polarization now gained by the L valleys due to our controlling trick presented above [it is shown in Fig. 5(e) that $P_L(0)$ can even be higher than 5 %]. Furthermore, there is no spin precession in L valleys anymore. It is further noted that the Γ - L inter-valley electron-phonon scattering is the dominant inter-valley scattering. This can be seen from Fig. 5(c) that in the presence of $H_{\Gamma-L}^{e-p}$ but in the absence of $H_{\Gamma-L}^{e-e}$, the spin polarization of L valleys shows the

same damping rate and precession period. This is because when the electric field is relatively low (here $E = 2$ kV/cm), only a small number of electrons distribute in L valleys [see the inset of Fig. 8(a)]. Therefore the inter-valley Coulomb scattering is very weak.

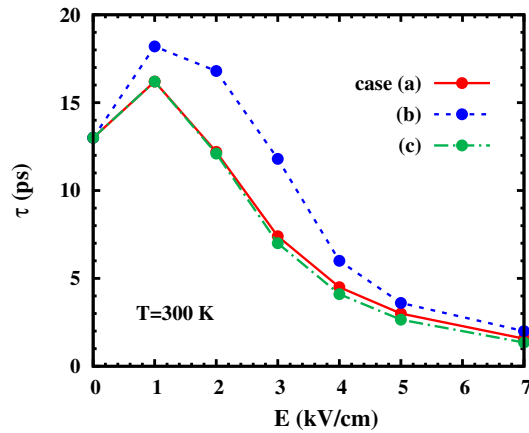


FIG. 6: (Color online) Spin relaxation time τ vs. electric field E . Solid curve: with both $H_{\Gamma-L}^{e-p}$ and $H_{\Gamma-L}^{e-e}$ [case (a)]; Dashed curve: without $H_{\Gamma-L}^{e-p}$ [case (b)]; Chain curve: without $H_{\Gamma-L}^{e-e}$ [case (c)]. $T = 300$ K and $N_i = B = 0$.

The above features can be well understood with respect to the different spin-orbit couplings in different valleys, in conjunction with the strong inter-valley scattering. The spin-orbit coupling strength of L valleys is about 16 times as large as that of Γ valley.⁴⁸ This strong inhomogeneous broadening leads to a fast spin decay in L valleys if they are isolated from Γ valley [see the dashed curve in Fig. 5(d), which has a corresponding spin relaxation time in the order of 0.1 ps]. Moreover, the fast spin relaxation of L valleys also manifests itself in the quick initial spin decay after turning on the coherent terms in Fig. 5(b-d), as shown in Fig. 5(e). It is therefore understood that due to the efficient inter-valley exchange of electrons caused by the inter-valley electron-phonon scattering as well as the large spin-orbit coupling in L valleys, L valleys play the role of a “drain” of spin polarization and enhance spin relaxation of the total system effectively [comparing the chain curves in Fig. 5(a) and Fig. 5(b)]. Meanwhile, the strong inter-valley electron-phonon scattering causes the spin evolutions of different valleys to be almost identical.

To have a further insight into the effect of inter-valley scattering on spin relaxation under different electric fields, the spin relaxation time τ against E is shown in Fig. 6 under conditions (a), (b) and (c) defined above. In the figure, the enhancement of spin relaxation caused by L valleys via inter-valley electron-phonon scattering is obvious by comparing the solid and dashed curves. The effect of inter-valley Coulomb scattering becomes visible when E is high (> 2 kV/cm), leading to a marginal decrease of the spin relaxation. That is because in the strong scattering limit, adding new scattering tends to

reduce the spin relaxation by its counter effect on inhomogeneous broadening.⁴⁷

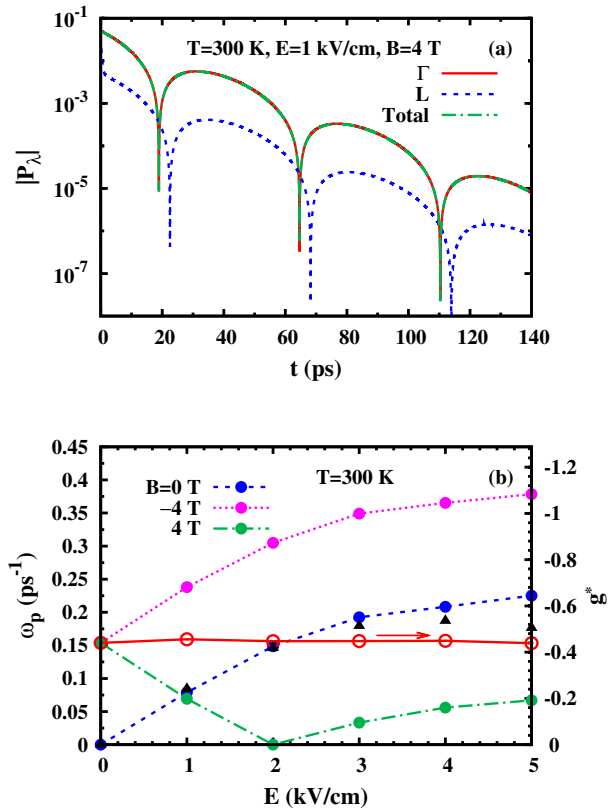


FIG. 7: (Color online) (a): Temporal evolution of $|P_\lambda|$ with electric field $E = 1$ kV/cm and magnetic field $B = 4$ T. (b): Spin precession frequency ω_p against electric field E when static magnetic field $B = 0$ T (dashed curve), -4 T (dotted curve) and 4 T (chain curve). Triangular dots: spin precession frequency under electric field predicted by Eq. 12 when $B = 0$ T. Solid curve: calculated effective g -factor g^* under different electric fields (note the scale of this curve is on the right hand side of the frame).

C. Spin precession

Now we turn to investigate the property of spin precession. It is known that in the presence of electric field, spins can precess under the electric-field-induced effective magnetic field.¹¹ When a static magnetic field is further applied, spins then precess around the combined effective magnetic field. We define the combined effective magnetic field term as $\Omega(\mathbf{B}) = \Omega_0 + \frac{1}{2}g^*\mu_B\mathbf{B}$. Here Ω_0 is the induced magnetic field term, which is dependent on the electric field. g^* is the effective g -factor. The corresponding spin precession frequency around $\Omega(\mathbf{B})$ is

$\omega_p \equiv 2|\Omega(\mathbf{B})|/\hbar$. For each valley,¹¹

$$\Omega_0^\lambda = \frac{\int d\mathbf{k}_\lambda (f_{\mathbf{k}_\lambda, \frac{1}{2}} - f_{\mathbf{k}_\lambda, -\frac{1}{2}}) \mathbf{h}_\lambda(\mathbf{k}_\lambda)}{\int d\mathbf{k}_\lambda (f_{\mathbf{k}_\lambda, \frac{1}{2}} - f_{\mathbf{k}_\lambda, -\frac{1}{2}})}. \quad (11)$$

From Eqs. (6) and (7), one finds immediately that for Γ valley, Ω_0^Γ is along the x -axis when the electric field is along the x -axis (note that $\langle k_{\Gamma z}^2 \rangle$ is larger than the mean value of $k_{\Gamma y}^2$ due to the strong confinement along the z -axis), while for L valleys, $\{\Omega_0^{L_i}\}$ share the same magnitude but direct along $(0, \pm 1, \pm 1)$ directions. Therefore there is no net induced magnetic field under electric field in L -valleys, i.e., $\sum_i \Omega_0^{L_i} = 0$ and Ω_0 of the whole system comes from Ω_0^Γ . A direct inferrer is that no spin precession will appear for electrons in L valleys under electric field only. However, as shown in Fig. 5(a), due to the strong Γ - L inter-valley scattering, spin precession in L valleys under electric field only is observed and shares the *same* precession period as the Γ valley. One may also expect that when a static magnetic field is applied, electron spins at L valleys may have a distinct spin precession frequency as the g -factor of L valley is three times as large as that of Γ valley. Nevertheless, again this is not the case. Due to both the strong inhomogeneous broadening (i.e., fast spin relaxation in L valleys) and the intensive exchange of electrons between Γ and L valleys due to the strong inter-valley scattering, L valleys still present the same precession period as that of Γ valley, as shown in Fig. 7(a). This is because electron spins in L valleys can hardly show any spin precession characterized by $g_L\mu_B B/2$ without being depolarized from the strong inhomogeneous broadening-induced interference decay as well as being scattered back to Γ valley due to the strong inter-valley scattering. (In fact, the spin precession time characterized by $g_L\mu_B B/2$ is 13.2 ps, the spin precession time under the momentum-dependent effective magnetic field from spin-orbit coupling in L valleys is around 0.2 ps and the L - Γ inter-valley electron-phonon scattering time calculated using Fermi's golden rule is about 0.4 ps when $T = 300$ K.) Therefore, the spin polarization in L valleys is just “pumped” from the Γ valley due to the strong inter-valley scattering. Consequently, the spin precession of the total system is determined by Γ valley. In the following, we prove this by exploring the effective g -factor of the total system.

The frequency of spin precession ω_p as function of electric field E is plotted in Fig. 7(b), in both the presence and absence of the applied magnetic field in Voigt configuration. It is shown that when the magnetic field is absent or is applied along $-x$ -axis direction, ω_p increases monotonically with the electric field. Nevertheless, when the magnetic field is along x -axis, ω_p first decreases to zero and then increases again with E . The monotonic increase in the absence of the magnetic field is due to the increase of the electric-field-induced magnetic field. In fact, when the spin polarization is small, in low electric field regime the induced magnetic field term Ω_0 can be

roughly estimated by Eq. (11) of Γ valley, i.e.,

$$\Omega_0 = \frac{\gamma m_{\Gamma}^2 v_{\Gamma}}{\hbar^3} \left[\frac{\varepsilon_F}{2(1 - e^{-\varepsilon_F/k_B T_{\Gamma}})} - \frac{\hbar^2 \pi^2}{2m_{\Gamma} a^2} \right]. \quad (12)$$

The spin precession frequency calculated using Eq. (12) in the absence of magnetic field is plotted as triangular dots in Fig. 7(b). It is seen that they coincide pretty well with the full calculation at low electric field regime. As the induced magnetic field is along $-x$ -axis, consequently an applied static magnetic field along $-x$ -axis increases the spin precession frequency universally by a constant number (comparing the dashed and dotted curves in the figure). However, when the applied magnetic field is along x -axis which is in opposite direction to the induced magnetic field, the induced magnetic field does not overcome the static magnetic field until the electric field is larger than 2 kV/cm. By utilizing the relation $-\frac{1}{2}g^*\mu_B B|_{B=4} = \Omega(0) - \Omega(4)$ (or $\frac{1}{2}g^*\mu_B B|_{B=-4} = \Omega(-4) - \Omega(0)$), one can get g^* under different electric fields. Simple calculations show that g^* changes little with electric field and is around the value when the electric field is absent, i.e., $g^* \approx g_{\Gamma} = -0.44$ [see the solid curve in Fig. 7 (b)], suggesting that the spin precession properties of the total system mainly come from electrons of Γ valley.

D. Effect of temperature, magnetic field, and impurity on spin relaxation

In this subsection we discuss the effect of temperature, magnetic field, and impurity on spin relaxation. Spin relaxation time τ against electric field E at different temperatures $T = 300, 200$ and 100 K with and without magnetic field/impurities are shown in Fig. 8.

From the figure one can see that in each case, the peak in τ - E curve (first discussed in Sec. IIIB) is more pronounced and shows up at a relatively higher electric field when T is decreased. This is due to two facts: First, the hot-electron effect mentioned previously in Sec. IIIA is more important when T is low.¹¹ Second, when temperature is low, the Γ - L inter-valley exchange of electrons in low electric field regime is marginal due to the low electron density in L valleys [see the inset of Fig. 8(a)]. Thus the enhancement of spin relaxation by L valleys does not come into effect markedly until the electric field is high enough.

It is also shown from the figure that in the low electric field regime ($E \leq 2$ kV/cm), the spin relaxation can be reduced by increasing temperature and/or magnetic field and/or impurity density. The reduction of the spin relaxation due to higher temperature and impurity density corresponds to the hot-electron effect in strong scattering limit—the increase of temperature and/or adding more impurities strengthen the scattering, thus reduce the spin R&D. The main effect of static magnetic field in the low electric field regime is to reduce the spin R&D by forcing

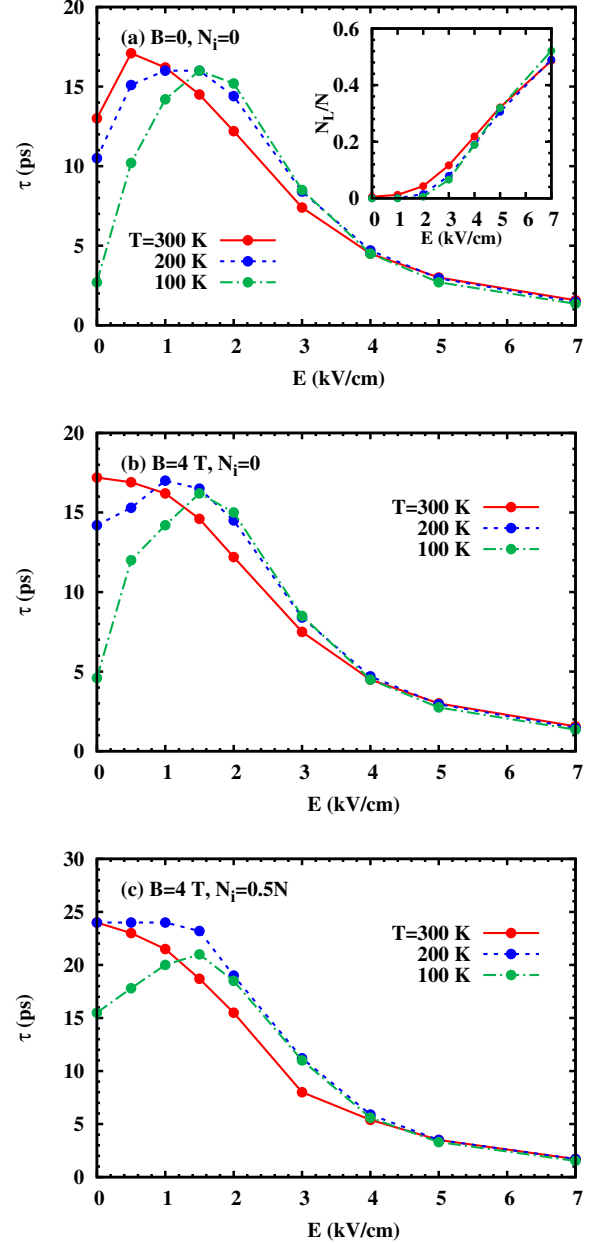


FIG. 8: (Color online) Spin relaxation time τ against electric field E when temperature $T=300$ (solid curves), 200 (dashed curves) and 100 K (chain curves) under different conditions: (a) $B = N_i = 0$; (b) $B = 4$ T and $N_i=0$; and (c) $B = 4$ T and $N_i = 0.5N$. Inset of (a): fraction of electrons in L valleys against electric field.

spins to undergo a Larmor precession around it and thus reducing inhomogeneous broadening.¹⁹

Finally one notices from the figure that when E is high enough, the effects of lattice temperature, impurity density, and magnetic field are marginal. In this regime, the inter-valley electron-phonon scattering is considerably strengthened due to the high hot-electron temperatures, and thus dominates and becomes insensitive to

the background temperature. Thus the changes in lattice temperature and other kinds of scattering cause little discrepancy in spin relaxation. Meanwhile, the inhomogeneous broadening is highly enhanced as well in this high electric field regime. Therefore the finite magnetic field has little restriction on inhomogeneous broadening and affects spin relaxation marginally. Consequently, the spin relaxation under high electric field tends to be identical and insensitive to the lattice temperature, magnetic field and impurity density.

IV. CONCLUSION

In conclusion, we investigate the multi-valley spin relaxation in *n*-type GaAs QWs in the presence of in-plane electric field under high temperature (≥ 100 K), by applying the KSBE approach. Due to the small well width in this investigation, electrons at Γ and L valleys determine the properties of spin dynamics at high electric field. We discuss the effect of inter-valley scattering on spin relaxation, the spin precession properties, and the spin relaxation under different conditions, such as lattice temperatures, magnetic fields and impurity densities.

First, the negative differential electric conductance, which is essential for the charge Gunn effect, is reproduced. Meanwhile, the hot-electron temperature is also investigated, showing that Γ valley has *two* distinct temperatures. One is for electrons in the energy regime which overlaps with that of L valleys, and shows the *same* hot-electron temperature of those in L valleys (T_L). The other is for electrons in the lower energy regime of Γ valley (T_Γ). It is shown that $T_\Gamma > T_L$. The identical electron temperature in the overlapped energy regime of Γ and L valleys is due to the strong inter-valley scattering whereas $T_\Gamma > T_L$ results from the smaller effective mass in Γ valley.

The spin relaxation time τ first increases and then decreases with the electric field, especially at low temperatures. The first increase of τ in low electric field regime is due to the hot-electron effect in the strong scattering limit. Whereas the following decrease of τ in the high electric field regime is mainly due to the fast spin relaxation in L valleys (originating from the much stronger spin-orbit coupling at L valleys) and strong Γ - L inter-valley scattering. In fact, L valleys are shown to play the role of a “drain” of the total spin polarization. It is also shown that the Γ - L inter-valley electron-phonon scattering is responsible for the inter-valley scattering. The contribution of Γ - L inter-valley electron-electron Coulomb scattering is marginal as it does not cause any electron exchange between different valleys. Moreover, due to the strong Γ - L inter-valley scattering as well as the strong inhomogeneous broadening in L valleys, electrons in L valleys possess almost the same spin relaxation rate and spin precession period as those in Γ valley. It is further shown that this feature still holds when a static magnetic field is applied. Actually, in our investigation ($B \leq 4$ T), the spin precession frequency is determined by elec-

trons at Γ valley, despite the fact that g_L is much larger in magnitude than g_Γ . This is because the net electric-field-induced magnetic field from L valleys is zero, and the effect of static magnetic field in L valleys can not surpass the much stronger inhomogeneous broadening as well as frequent exchange of electrons from Γ valley.

We also investigate the effects of temperature, magnetic field and impurity on spin relaxation. When the electric field is not too high, the spin relaxation can be reduced by increasing temperature, magnetic field, and impurity density. However, when the electric field is high enough, spin relaxation time is dominated by the Γ - L inter-valley electron-phonon scattering and becomes insensitive to temperature, impurity density and magnetic field.

Finally we remark on the possibility of the “spin Gunn effect” in GaAs QWs. First, as pointed out in our previous work,⁴⁹ the feasibility of drift-diffusion model used in Ref. 34 is valid only in system without Dresselhaus/Rashba spin-orbit coupling. For Zinc-blende semiconductors, even without magnetic field, electron spins can flip due to the Dresselhaus/Rashba spin-orbit coupling, let alone an effective magnetic field induced by electric field via the same spin-orbit coupling. Therefore, although with the spin-dependent mobilities, electrons with opposite spins can experience frequent spin-flip. Second, our calculations show that in high electric field regime, spin relaxation time decreases effectively with electric field. This is due to the hot-electron effect, together with the fast spin relaxation in the upper valleys. Therefore, the condition for “spin Gunn effect” proposed in Ref. 34 can hardly be realized due to the short spin relaxation time in GaAs QWs.

Acknowledgments

This work was supported by the Natural Science Foundation of China under Grant Nos. 10574120 and 10725417, the National Basic Research Program of China under Grant No. 2006CB922005 and the Knowledge Innovation Project of Chinese Academy of Sciences. One of the authors (P.Z.) would like to thank M. Q. Weng and J. H. Jiang for valuable discussions.

APPENDIX A: THE COHERENT AND SCATTERING TERMS OF THE KSBEs

The coherent terms are

$$\dot{\rho}_{\mathbf{k}_\lambda}|_{coh} = -i[\boldsymbol{\Omega}_\lambda(\mathbf{k}_\lambda) \cdot \boldsymbol{\sigma} - \sum_{\mathbf{q}} V_{\lambda\lambda,\mathbf{q}} \rho_{\mathbf{k}_\lambda-\mathbf{q}} \rho_{\mathbf{k}_\lambda}], \quad (\text{A1})$$

with $\boldsymbol{\Omega}_\lambda(\mathbf{k}_\lambda) \equiv \mathbf{h}_\lambda(\mathbf{k}_\lambda) + \frac{1}{2}g_\lambda\mu_B\mathbf{B}$ and $V_{\lambda\lambda,\mathbf{q}}$ representing the intra-valley Coulomb scattering matrix element. $[A, B]$ stands for the commutator of A and B . The scattering terms are

$$\rho_{\mathbf{k}_\lambda}^{\text{scat}, \lambda\lambda'} = -\{S_{\lambda\lambda'}^{\mathbf{k}_\lambda}(>, <) - S_{\lambda\lambda'}^{\mathbf{k}_\lambda}(<, >) + S_{\lambda\lambda'}^{\mathbf{k}_\lambda}(>, <)^\dagger - S_{\lambda\lambda'}^{\mathbf{k}_\lambda}(<, >)^\dagger\}, \quad (\text{A2})$$

where

$$\begin{aligned} S_{\lambda\lambda'}^{\mathbf{k}_\lambda}(>, <) &= \pi N_i \delta_{\lambda\lambda'} \sum_{\mathbf{q}} U_{\lambda\lambda, \mathbf{q}}^2 \rho_{\mathbf{k}_\lambda - \mathbf{q}}^> \rho_{\mathbf{k}_\lambda}^< \delta(\varepsilon_{\mathbf{k}_\lambda} - \varepsilon_{\mathbf{k}_\lambda - \mathbf{q}}) \\ &+ \pi \sum_{\mathbf{q}, \mathbf{k}'_\lambda} V_{\lambda\lambda', \mathbf{q}}^2 \rho_{\mathbf{k}_\lambda - \mathbf{q}}^> \rho_{\mathbf{k}'_\lambda}^< \text{Tr}[\rho_{\mathbf{k}'_\lambda}^> \rho_{\mathbf{k}'_\lambda - \mathbf{q}}^<] \delta(\varepsilon_{\mathbf{k}_\lambda - \mathbf{q}} - \varepsilon_{\mathbf{k}_\lambda} + \varepsilon_{\mathbf{k}'_\lambda} - \varepsilon_{\mathbf{k}'_\lambda - \mathbf{q}}) \\ &+ \pi \sum_{\mathbf{k}'_\lambda} M_{\lambda\lambda', \mathbf{q}}^2 \rho_{\mathbf{k}'_\lambda}^> \rho_{\mathbf{k}_\lambda}^< [N_{\lambda\lambda'}^< \delta(\varepsilon_{\mathbf{k}_\lambda} - \varepsilon_{\mathbf{k}'_\lambda} - \Omega_{\lambda\lambda'}) + N_{\lambda\lambda'}^> \delta(\varepsilon_{\mathbf{k}_\lambda} - \varepsilon_{\mathbf{k}'_\lambda} + \Omega_{\lambda\lambda'})]. \end{aligned} \quad (\text{A3})$$

Here $\rho_{\mathbf{k}}^< = \rho_{\mathbf{k}}$ and $\rho_{\mathbf{k}}^> = 1 - \rho_{\mathbf{k}}$. $N_{\lambda\lambda'} = N_{\lambda'\lambda} = [\exp(\hbar\Omega_{\lambda\lambda'}/k_B T) - 1]^{-1}$ is the Bose distribution of phonons with frequency $\Omega_{\lambda\lambda'}$. $N_{\lambda\lambda'}^< = N_{\lambda\lambda'}$ and $N_{\lambda\lambda'}^> = 1 + N_{\lambda\lambda'}$. $M_{\lambda\lambda', \mathbf{q}}$ is the matrix element of electron-phonon scattering with $\mathbf{q} = \mathbf{k}_\lambda - \mathbf{k}'_\lambda + \mathbf{k}_\lambda^0 - \mathbf{k}'_\lambda^0$ being the two-dimensional phonon wave vector. The intra-valley electron-acoustic-phonon scattering is neglected in the present investigation due to the high temperature. The matrix elements of the intra-valley electron-longitudinal-optical (LO) phonon scattering in Γ valley and the intra-valley optical-phonon deformation potential scattering in L valleys are given by $M_{\Gamma\Gamma, \mathbf{q}}^2 = \sum_{q_z} \frac{e^2 \hbar \Omega_{\Gamma\Gamma}}{2\varepsilon_0(q^2 + q_z^2)} (\kappa_\infty^{-1} - \kappa_0^{-1}) |I_{\Gamma\Gamma}(iq_z)|^2$ and $M_{L_i L_i, \mathbf{q}}^2 = \sum_{q_z} \frac{\hbar D_{L_i L_i}^2}{2d\Omega_{L_i L_i}} |I_{L_i L_i}(iq_z)|^2$, respectively.²⁸ For the inter-valley electron-phonon scattering, selection rules applied to a cubic zinc-blende structure of III-V semiconductors show that the LO and longitudinal-acoustic (LA) phonons can assist the inter-valley transitions.⁵⁰ However, it was further shown later that the selection rules do not apply in the high energy regime where the inter-valley transfer can happen.^{51,52,53} Therefore, all phonon branches including transverse optical (TO) and transverse acoustic (TA) phonons can contribute to the inter-valley scattering.⁵³ Nevertheless, the electron-TA phonon scattering is very weak and can be neglected.^{51,53} The LO, TO and LA phonons have comparable energies,⁵² thus the inter-valley scattering can be considered by grouping together the scattering assisted by these phonons and using the average phonon energy and the total coupling constant.⁵³ Here the two-dimensional phonon wave vector \mathbf{q} is mainly determined by the large component $\mathbf{k}_\lambda^0 - \mathbf{k}'_\lambda^0$, thus the average phonon energy and the total coupling constant are approximated to be fixed. Therefore, we have $M_{\Gamma L_i, \mathbf{q}}^2 = M_{L_i \Gamma, \mathbf{q}}^2 = \sum_{q_z} \frac{\hbar D_{\Gamma L_i}^2}{2d\Omega_{\Gamma L_i}} |I_{\Gamma L_i}(iq_z)|^2$ for Γ - L inter-valley electron-phonon scattering, and $M_{L_i L_j, \mathbf{q}}^2 = \sum_{q_z} \frac{\hbar D_{L_i L_j}^2}{2d\Omega_{L_i L_j}} |I_{L_i L_j}(iq_z)|^2$ for L - L inter-valley electron-phonon scattering. Here $d = 5.36 \text{ g/cm}^3$ is the mass density of the crystal; $\kappa_0 = 12.9$ and $\kappa_\infty = 10.8$ are the relative static and high-frequency dielectric

constants respectively; ε_0 is the vacuum dielectric constant. The phonon energies are $\hbar\Omega_{\Gamma\Gamma} = 35.4 \text{ meV}$, $\hbar\Omega_{L_i L_i} = 34.3 \text{ meV}$,²⁸ $\hbar\Omega_{\Gamma L_i} = \hbar\Omega_{L_i \Gamma} = 20.8 \text{ meV}$,²⁸ and $\hbar\Omega_{L_i L_j} = 29.0 \text{ meV}$.²⁸ The deformation potentials are $D_{L_i L_i} = 0.3 \times 10^9 \text{ eV/cm}$,²⁸ $D_{\Gamma L_i} = 1.1 \times 10^9 \text{ eV/cm}$,^{28,53} and $D_{L_i L_j} = 1.0 \times 10^9 \text{ eV/cm}$.^{28,53} $V_{\lambda\lambda', \mathbf{q}} = \sum_{q_z} \frac{e^2}{\varepsilon_0 \kappa_0 (q^2 + q_z^2 + \kappa^2)} I_{\lambda\lambda}(iq_z) I_{\lambda'\lambda'}^*(iq_z) = \sum_{q_z} \frac{e^2}{\varepsilon_0 \kappa_0 (q^2 + q_z^2 + \kappa^2)} |I_{\lambda\lambda}(iq_z)|^2$ is the intra-valley (inter-valley) Coulomb scattering matrix element when $\lambda = \lambda'$ ($\lambda \neq \lambda'$). $U_{\lambda\lambda, \mathbf{q}}^2 = \sum_{q_z} \{Z_i e^2 / [\varepsilon_0 \kappa_0 (q^2 + q_z^2 + \kappa^2)]\}^2 |I_{\lambda\lambda}(iq_z)|^2$ is the intra-valley electron-impurity scattering potential, with $Z_i = 1$ being the charge number of the impurity. N_i is the impurity density. $\kappa^2 = Ne^2 / (\varepsilon_0 \kappa_0 k_B T)$ is the screening constant. The form factor $|I_{\lambda\lambda'}(iq_z)|^2 \equiv |\langle \phi_\lambda(z) | e^{iq_z z} | \phi_{\lambda'}(z) \rangle|^2 = \frac{\pi^4 \sin^2 y}{y^2 (y^2 - \pi^2)^2}$ with $y \equiv a(q_z - K_{\lambda z}^0 + K_{\lambda' z}^0)/2$.

APPENDIX B: NUMERICAL SCHEME

We extend the numerical scheme for solving the KSBEs at Γ valley only, shown in detail in Ref. 11, to the case with both Γ and L valleys. To do so, five circular zones centered at the bottom of each valley in momentum space are set up. We divide the truncated two-dimensional momentum space in Γ valley into $N_\Gamma \times M$ control regions, and that in L_i ($i=1, \dots, 4$) valley into $N_{L_i} \times M$ control regions. The relative \mathbf{k}_λ -grid point in λ valley is chosen to be the center of the region,

$$\mathbf{k}_\lambda^{n,m} = \frac{\sqrt{2m_\lambda E_n^\lambda}}{\hbar} (\cos \theta_m, \sin \theta_m), \quad (\text{B1})$$

with $E_n^\lambda = (n + 0.5)\Delta E$ and $\theta_m = m\Delta\theta$ ($n=0, 1, \dots, N_{cut}^\lambda - 1$ and $m=0, 1, \dots, M - 1$). Here $N_{cut}^\Gamma = N_\Gamma$ for Γ valley and $N_{cut}^{L_i} = N_{L_i}$ for L valleys. The truncation energy is $E_{N_{cut}^\lambda}^\lambda$. Due to the effective Γ - L energy difference, $E_{N_\Gamma - 1}^\Gamma - E_{N_{L_i} - 1}^{L_i} = \varepsilon_{\Gamma L}$. Thus N_Γ and N_{L_i} are chosen to satisfy $N_\Gamma - N_{L_i} = \lfloor \frac{\varepsilon_{\Gamma L}}{\Delta E} \rfloor$ ($\lfloor \frac{\varepsilon_{\Gamma L}}{\Delta E} \rfloor$ is the integer part of $\frac{\varepsilon_{\Gamma L}}{\Delta E}$). The energy partition ΔE is set

as $\hbar\Omega_{\Gamma}/n_{LO}$ with n_{LO} being an integer, and the angle partition is $\Delta\theta = 2\pi/M$. The coherent terms and the scattering terms of electron-impurity scattering can be discretized directly. By virtue of the chosen energy partition, intervalley electron-phonon scattering in Γ valley can be discretized immediately as well. For intra-valley electron-phonon scattering in L valleys and inter-valley

electron-phonon scattering, one expects to have the energy difference be the integer multiplication of ΔE . This is difficult to satisfy in general. However, with an optimal value of n_{LO} , one can approximately achieve above requirement. The remaining numerical scheme is all the same as those given in Ref. 11.

-
- * Author to whom correspondence should be addressed; Electronic address: mwwu@ustc.edu.cn.
- ¹ F. Meier and B. P. Zakharchenya, *Optical Orientation* (North-Holland, Amsterdam, 1984).
 - ² D. D. Awschalom, D. Loss, and N. Samarth, *Semiconductor Spintronics and Quantum Computation* (Springer, Berlin, 2002).
 - ³ I. Žutić, J. Fabian, and S. D. Sarma, *Rev. Mod. Phys.* **76**, 323 (2004); J. Fabian, A. Matos-Abiague, C. Ertler, P. Stano, and I. Žutić, *acta physica slovaca* **57**, 565 (2007).
 - ⁴ Y. A. Bychkov and E. I. Rashba, *Zh. Éksp. Teor. Fiz.* **39**, 66 (1984) [*JETP Lett.* **39**, 78 (1984)].
 - ⁵ Y. A. Bychkov and E. I. Rashba, *J. Phys. C: Solid State Phys.* **17**, 6039 (1984).
 - ⁶ J. Nitta, F. E. Meijer, and H. Takayanagi, *Appl. Phys. Lett.* **75**, 695 (1999).
 - ⁷ Y. Kato, R. C. Myers, A. C. Gossard, and D. D. Awschalom, *Nature* **427**, 50 (2004).
 - ⁸ L. Jiang and M. W. Wu, *Phys. Rev. B* **72**, 033311 (2005).
 - ⁹ S. A. Crooker and D. L. Smith, *Phys. Rev. Lett.* **94**, 236601 (2005); M. Hruška, Š. Kos, S. A. Crooker, A. Saxena, and D. L. Smith, *Phys. Rev. B* **73**, 075306 (2006).
 - ¹⁰ M. Beck, C. Metzner, S. Malzer, and G. H. Döhler, *Europhys. Lett.* **75**, 597 (2006).
 - ¹¹ M. Q. Weng, M. W. Wu, and L. Jiang, *Phys. Rev. B* **69**, 245320 (2004).
 - ¹² S. Pramanik, S. Bandyopadhyay, and M. Cahay, *Phys. Rev. B* **68**, 075313 (2003).
 - ¹³ S. Pramanik, S. Bandyopadhyay, and M. Cahay, *Appl. Phys. Lett.* **84**, 266 (2004).
 - ¹⁴ E. A. Barry, A. A. Kiselev, and K. W. Kim, *Appl. Phys. Lett.* **82**, 3686 (2003).
 - ¹⁵ M. W. Wu and C. Z. Ning, *Eur. Phys. J. B* **18**, 373 (2000); M. W. Wu, *J. Phys. Soc. Jpn.* **70**, 2195 (2001).
 - ¹⁶ M. M. Glazov and E. L. Ivchenko, *Pis'ma Zh. Eksp. Teor. Fiz.* **75**, 476 (2002) [*JETP Lett.* **75**, 403 (2002)].
 - ¹⁷ M. W. Wu and H. Metiu, *Phys. Rev. B* **61**, 2945 (2000).
 - ¹⁸ M. W. Wu, M. Q. Weng, and J. L. Cheng, in *Physics, Chemistry and Application of Nanostructures: Reviews and Short Notes to Nanomeeting 2007*, edited by V. E. Borisenko, V. S. Gurin, and S. V. Gaponenko (World Scientific, Singapore, 2007), pp. 14, and references therein.
 - ¹⁹ M. Q. Weng and M. W. Wu, *Phys. Rev. B* **68**, 075312 (2003).
 - ²⁰ M. Q. Weng and M. W. Wu, *Phys. Rev. B* **70**, 195318 (2004).
 - ²¹ J. Zhou, J. L. Cheng, and M. W. Wu, *Phys. Rev. B* **75**, 045305 (2007).
 - ²² M. A. Brand, A. Malinowski, O. Z. Karimov, P. A. Marsden, R. T. Harley, A. J. Shields, D. Sanvitto, D. A. Ritchie, and M. Y. Simmons, *Phys. Rev. Lett.* **89**, 236601 (2002); W. J. H. Leyland, G. H. John, R. T. Harley, M. M. Glazov, E. L. Ivchenko, D. A. Ritchie, I. Farrer, A. J. Shields, and M. Henini, *Phys. Rev. B* **75**, 165309 (2007).
 - ²³ D. Stich, J. Zhou, T. Korn, R. Schulz, D. Schuh, W. Wegscheider, M. W. Wu, and C. Schüller, *Phys. Rev. Lett.* **98**, 176401 (2007); *Phys. Rev. B* **76**, 205301 (2007).
 - ²⁴ D. Stich, T. Korn, R. Schulz, D. Schuh, W. Wegscheider, and C. Schüller, *Physica E* **40**, 1545 (2008).
 - ²⁵ A. P. Dmitriev, V. Y. Kachorovskii, M. S. Shur, and M. Stroschio, *Solid State Commun.* **113**, 565 (2000).
 - ²⁶ A. W. Holleitner, V. Sih, R. C. Myers, A. C. Gossard, and D. D. Awschalom, *New J. Phys.* **9**, 342 (2007).
 - ²⁷ J. B. Gunn, *Solid State Commun.* **1**, 88 (1963).
 - ²⁸ X. L. Lei, D. Y. Xing, M. Liu, C. S. Ting, and J. L. Birman, *Phys. Rev. B* **36**, 9134 (1987).
 - ²⁹ D. Y. Xing, M. Liu, and C. S. Ting, *Phys. Rev. B* **37**, 10283 (1987).
 - ³⁰ W. Magnus, C. Sala, and K. D. Meyer, *Phys. Rev. B* **43**, 9045 (1990).
 - ³¹ J. L. Educato, J. P. Leburton, J. Wang, and D. W. Bailey, *Phys. Rev. B* **44**, 8365 (1991).
 - ³² J. Sjakste, V. Tyuterev, and N. Vast, *Appl. Phys. A* **86**, 301 (2007).
 - ³³ S. Saikin, M. Shen, and M. C. Cheng, *J. Phys.: Condens. Matter* **18**, 1535 (2006).
 - ³⁴ Y. Qi, Z. G. Yu, and M. E. Flatté, *Phys. Rev. Lett.* **96**, 026602 (2006).
 - ³⁵ M. I. D'yakonov and V. I. Perel', *Zh. Éksp. Teor. Fiz.* **60**, 1954 (1971) [*Sov. Phys. JETP* **33**, 1053 (1971)].
 - ³⁶ N. Chand, T. Henderson, J. Klem, W. T. Masselink, and R. Fischer, *Phys. Rev. B* **30**, 4481 (1984).
 - ³⁷ J. Pozela and A. Reklaitis, *Solid State Commun.* **27**, 1073 (1978).
 - ³⁸ *Semiconductors*, Landolt-Börnstein, New Series, Vol. 17a, edited by O. Madelung (Springer, Berlin, 1987).
 - ³⁹ K. Shen, M. Q. Weng, and M. W. Wu, arXiv:0806.1252.
 - ⁴⁰ G. Dresselhaus, *Phys. Rev.* **100**, 580 (1955).
 - ⁴¹ E. L. Ivchenko and G. E. Pikus, *Superlattices and Other Heterostructures: Symmetry and Optical Phenomena* (Springer, Berlin, 1997).
 - ⁴² A. G. Aronov, G. E. Pikus, and A. N. Titkov, *Zh. Eksp. Teor. Fiz.* **84**, 1170 (1983) [*Sov. Phys. JETP* **57**, 680 (1983)].
 - ⁴³ J. Y. Fu, M. Q. Weng, and M. W. Wu, *Physica E* **40**, 2890 (2008).
 - ⁴⁴ G. D. Mahan, *Many-Particle Physics* (Plenum, New York, 1981).
 - ⁴⁵ H. Haug and A. P. Jauho, *Quantum kinetics in Transport and Optics of Semiconductors* (Springer, Berlin, 1998).
 - ⁴⁶ M. Liu, D. Y. Xing, C. S. Ting, and W. T. Xu, *Phys. Rev. B* **37**, 2997 (1988).
 - ⁴⁷ C. Lü, J. L. Cheng, and M. W. Wu, *Phys. Rev. B* **73**, 125314 (2006).

- ⁴⁸ By comparing the coefficients of first order term of \mathbf{k}_λ in Eqs. (6) and (7), one has $(\beta/\sqrt{3})/(\pi^2\gamma/2a^2) \approx 15.6$.
- ⁴⁹ M. Q. Weng and M. W. Wu, Phys. Rev. B **66**, 235109 (2002).
- ⁵⁰ J. L. Birman, M. Lax and R. Loudon, Phys. Rev. **145**, 620 (1966).
- ⁵¹ D. C. Herbert, J. Phys. C: Solid State Phys. **6**, 2788 (1973).
- ⁵² W. Fawcett and D. C. Herbert, J. Phys. C: Solid State Phys. **7**, 1641 (1974).
- ⁵³ R. Mickevičius and A. Reklaitis, J. Phys.: Condens. Matter **2**, 7883 (1990).